



RESEARCH ARTICLE

10.1029/2021MS002475

Development and Implementation of a Physics-Based Convective Mixing Scheme in the Community Multiscale Air Quality Modeling Framework

Key Points:

- Implemented a more physically accurate convection mixing model based on Kain and Fritsch scheme into Community Multiscale Air Quality (CMAQ) modeling
- Investigated the convection model on the vertical and spatial distribution of air pollutants over East Asia using CMAQ modeling
- Two convective transport impacts: (a) direct impact by vertical convective fluxes and (b) indirect impact originating from vertical fluxes

Arman Pouyaei¹ , Bavand Sadeghi¹ , Yunsoo Choi¹ , Jia Jung¹ , Amir H. Souri² , Chun Zhao^{3,4} , and Chul Han Song⁵

¹Department of Earth and Atmospheric Sciences, University of Houston, Houston, TX, USA, ²Harvard-Smithsonian Center for Astrophysics, Cambridge, MA, USA, ³School of Earth and Space Sciences, University of Science and Technology of China, Hefei, China, ⁴CAS Center for Excellence in Comparative Planetology, University of Science and Technology of China, Hefei, China, ⁵School of Environmental Science and Engineering, Gwangju Institute of Science and Technology, Gwangju, South Korea

Supporting Information:

Supporting Information may be found in the online version of this article.

Correspondence to:

Y. Choi,
ychoi6@uh.edu

Citation:

Pouyaei, A., Sadeghi, B., Choi, Y., Jung, J., Souri, A. H., Zhao, C., & Song, C. H. (2021). Development and implementation of a physics-based convective mixing scheme in the community multiscale air quality modeling framework. *Journal of Advances in Modeling Earth Systems*, 13, e2021MS002475. <https://doi.org/10.1029/2021MS002475>

Received 20 JAN 2021

Accepted 29 MAY 2021

Abstract To improve the representation of convective mixing of atmospheric pollutants in the presence of clouds, we developed a convection module based on Kain and Fritsch (KF) method and implemented it in the Community Multiscale Air Quality model. The KF-convection method is a mass-flux-based model that accounts for updraft flux, downdraft flux, entrainment, detrainment, and the subsidence effect. The method is consistent with the convection parametrization of the meteorology model. We apply the KF-convection model to an idealized case and to a reference setup prepared for East Asia during the KORUS-AQ campaign period to investigate its impact on carbon monoxide (CO) concentration at various atmospheric altitudes. We investigate the impact of KF-convection on the horizontal distribution of CO concentrations by comparing it to aircraft measurements and the MOPITT CO column. We further discuss two types of impacts of KF-convection: the direct impact caused by vertical movement of CO concentrations by updraft or downdraft and the indirect impact caused by transport of lifted CO concentrations to another region. May 12 saw a high indirect impact originating from the Shanghai region at higher altitudes and a high direct impact of updraft fluxes at 1 km altitude. However, May 26 revealed an immense updraft increasing higher altitude concentrations (up to 40 ppbv) and diverse indirect impacts over the region of the study (± 50 ppbv). The overall comparison shows a strong connection between differences in the amount of concentration caused by the direct impact at each altitude with the presence of an updraft at that altitude. The developed model can be employed in large domains (i.e., East Asia, Europe, North America, and Northern Hemisphere) with sub-grid scale cloud modeling to include the impacts of convection.

Plain Language Summary We developed a more physically accurate convective mixing model based on the Kain and Fritsch scheme for a chemical transport model. We verified the physical processes involved in the developed scheme for an idealized case and then implemented it into the Community Multiscale Air Quality modeling platform. We also investigated the developed convection model on the vertical and spatial distribution of carbon monoxide over East Asia during the KORUS-AQ aircraft campaign. We investigated the impact by comparing the results of these models to aircraft measurements and satellite retrievals. Furthermore, we separated the impact of convective transport over the study region into two types: the direct impact caused by vertical convective fluxes, which changed the vertical distribution of concentrations, and the indirect impact originating from vertical fluxes in neighboring regions and leading to spatial differences on vertical layers in the region of study. The developed model can be employed in large domains (i.e., East Asia, Europe, North America, and Northern Hemisphere) with sub-grid scale cloud modeling to include the convection impacts.

1. Introduction

Clouds have profound impacts on the Earth's atmosphere. They shape the characteristics of aerosols and greenhouse gases and elucidate a number of mechanisms that affect global and regional climate (Bogen-schutz et al., 2012; Wallace & Hobbs, 2006; Wu & Li, 2008). Cloud convection can transport gaseous and

© 2021. The Authors. Journal of Advances in Modeling Earth Systems published by Wiley Periodicals LLC on behalf of American Geophysical Union. This is an open access article under the terms of the [Creative Commons Attribution-NonCommercial-NoDerivs License](https://creativecommons.org/licenses/by-nc-nd/4.0/), which permits use and distribution in any medium, provided the original work is properly cited, the use is non-commercial and no modifications or adaptations are made.

particulate matter from the boundary layer into the free troposphere, redistribute these constituents, and return them back to the surface through dry and wet deposition processes (Stocker et al., 2013). The vertical distribution of pollutants among the convective layers and the roles it likely plays in surface layers' concentrations made it crucial for chemical transport models (CTMs) that convection schemes should be developed as one of the components of their framework. As the processes involved in convection impacts chemical constituents, physical descriptions of the clouds are essential for the understanding of the amount and composition of trace species in the atmosphere (Bogenschutz et al., 2012; Fahey et al., 2017; Seinfeld & Pandis, 2016). Nevertheless, researchers have encountered several challenges in the quest to explain the convective processes that take place within clouds (Barth et al., 2007; Ervens, 2015; Scott, 1981). A major challenge that lies at the core of our understanding has been how to represent the impacts of deep and shallow convections on gas-phase chemistry, wet deposition, and especially the distribution of atmospheric constituents (Fowler et al., 2020). Over the past decades, several studies have proposed various schemes of parameterizations to model the impacts of cloud convection for both regional and global models (Alapay et al., 2012; Arakawa, 2004; Byun & Schere, 2006; Herwehe et al., 2014; Randall et al., 2007) or to investigate cloud-aerosol-interaction modeling (Chapman et al., 2009; Grell et al., 2011). The results stemming from these parametrizations, however, are mostly inconsistent due to variability in assumptions and simplifications of the schemes (Heikenfeld et al., 2019; Lawrence & Rasch, 2005).

Cloud convection is typically composed of multiple processes, including updrafts carrying masses of air from lower levels to upper levels and downdrafts transporting masses of upper air to the surface, both of which affect the fluxes of masses in a group of layers in the atmosphere. Other processes taking place in cloud convection are entrainment, drawing of air masses into an updraft-downdraft plume, and detrainment, dispersion of masses out of an updraft-downdraft plume. Near tropical regions, the combination of convective processes increases the vertical transport of pollutants, causing a connection between surface emissions and the upper troposphere (Chandra et al., 2016). Several studies have highlighted the importance of deep-shallow convection in the transport of atmospheric constituents such as carbon monoxide (CO) in low to high-tropospheric altitudes (Erukhimova & Bowman, 2006; Ghude et al., 2011; Park et al., 2009; Yang et al., 2018). Therefore, to accurately simulate atmospheric chemistry over multiple vertical layers and correctly quantify long-range transport (Pouyaei et al., 2020; Tsai & Wu, 2017), a reliable convection scheme has been of atmospheric chemists and physicists communal tasks (Orbe et al., 2017; Yang et al., 2020).

Convective transport of chemical species in regional models is classified in clouds of full-grid and sub-grid scales. The EPA's Community Multiscale Air Quality (CMAQ) model (Byun & Schere, 2006) resolves the full-grid clouds that occupy the entire grid cell by the meteorological models and the parametrized sub-grid clouds. Among the convective parameterization schemes developed over the last decades, the algorithm of Kain-Fritsch (Kain & Fritsch, 1990, 1993) is one of the most physically accurate mass-flux parameterizations which has been used in multiple mesoscale and regional models (Saito et al., 2006; Samuelsson et al., 2011; Skamarock et al., 2005; Zhao et al., 2009, 2013). Although the latest version of the Kain-Fritsch scheme contains the essential physics to parametrize the convection, any version that follows must address several shortcomings such as the interactions between clouds, scale separation in deep convective clouds, and the interaction between microphysics and cloud radiation (Arakawa, 2004; Bechtold et al., 2001). In addition, similar to other cumulus parameterization methods, the Kain-Fritsch scheme entails uncertainty in the modeling of horizontally nonlocal structures (Arakawa, 2004; Ong et al., 2017; Sakradzija & Klocke, 2018). Although the CMAQ modeling framework addresses the issue of nonlocal structures by separating resolved clouds and sub-grid scale clouds, it still lacks physical efficacy when modeling convective mixing in clouds (Roselle & Binkowski, 1999). Moreover, the sub-grid convection in CTMs needs to be consistent with the cloud parametrization in the meteorological model (Li et al., 2018).

In this study, we introduce a modified version of the Kain-Fritsch scheme (Kain, 2004) and implement it into the CMAQ model to accomplish two objectives: (a) to develop a more physically accurate scheme of sub-grid cloud parameterization and (b) to enhance the capabilities of the CMAQ model to simulate the vertical distributions of chemical species in the layers of the atmosphere where convection has occurred. We also investigate the impact of KF-convection over the East Asia region during the KORUS-AQ campaign period by separately studying the convective mixing in vertical atmospheric layers and transported constituents caused by convection in the region of study using the Process Analysis (PA) approach.

2. Methodology

The original Kain and Fritsch (KF) scheme was derived and developed from the Fritsch-Chapel convective parametrization scheme (Fritsch & Chappell, 1980). In the 1990s, KF made a series of changes and introduced a more distinguishable scheme from its parent algorithm. The KF scheme of convection is a mass flux parameterization scheme that has been used in several Numerical Weather Prediction systems, including the Weather Research and Forecasting (WRF) model. Since the main goal of this study is to incorporate a cloud convection scheme into a CTM, we will describe in detail the methodology, we used to apply the concept of the KF scheme into vertical convective mixing of sub-grid cloud module in the CMAQ modeling platform. We chose the WRF-CMAQ two-way coupled model for this implementation, as it is more straightforward when transferring variables from WRF into CMAQ, and we can pass the variables in smaller intervals. We turned off the feedback of the system so that it will be the same as the offline WRF-CMAQ framework. In this section, we will provide a scientific description of the CMAQ model of cloud convection and present the implementation of KF convective mixing in the WRF-CMAQ framework.

2.1. Description of the Standard CMAQ Cloud Model

To understand the implementation of KF-convection in CMAQ, we will briefly review how the standard CMAQ (Standard-CMAQ) model processes convective mixing in the clouds. CMAQ accounts for cloud modeling in two main components of the sub-grid cloud model (subcld) and the resolved cloud model (rescld) (Roselle & Binkowski, 1999). The first component of the CMAQ model of the cloud takes into account smaller than grid size clouds, referred to as “sub-grid clouds.” The second component of the CMAQ cloud model simulates clouds that occupy the entire grid cell. The impacts of the latter, referred to as “rescld clouds,” have already been resolved by the meteorological model. The sub-grid and resolved cloud models update pollutant concentrations following the equation below, where \bar{m}_i represents pollutant concentrations:

$$\left. \frac{\partial \bar{m}_i}{\partial t} \right|_{\text{cld}} = \left. \frac{\partial \bar{m}_i}{\partial t} \right|_{\text{subcld}} + \left. \frac{\partial \bar{m}_i}{\partial t} \right|_{\text{rescld}}. \quad (1)$$

The scheme of rescld cloud utilized the meteorological model outputs for the impacts of the grid fully covered by clouds. The sub-grid scheme of CMAQ version 5.2 was inherited from the diagnostic cloud model of the Regional Acid Deposition Model version 2.6 (Chang et al., 1987; Dennis et al., 1993; Walcek & Taylor, 1986). This scheme parameterizes the convective effects of clouds by modeling a series of processes that include mixing, scavenging, aqueous chemistry, and wet deposition. These parameterizations assume that the area of cloud convection is smaller than the size of the grid cell. While the impacts of sub-grid clouds are updated once per hour, those of resolved clouds are updated at every synchronization time step. Hence, the CMAQ cloud module differentiated between sub-grid and resolved clouds both temporally and spatially. We applied the developed KF-convection scheme for every synchronization time step of sub-grid clouds only because the cumulus scheme modeling used in WRF simulates the impacts of resolved clouds. The application of KF-convection at every synchronization time step of CMAQ requires a more scientific understanding of the physical description of the Standard-CMAQ model of sub-grid clouds.

The sub-grid scheme of the cloud determines whether a cloud is precipitating or nonprecipitating. For precipitating clouds, CMAQ uses the amount of convective precipitation from the meteorological model. Nonprecipitating clouds are modeled when the relative humidity of the source level is above 70% and the calculated cloud base is below a certain level (Dennis et al., 1993). In both types of precipitating and nonprecipitating clouds, the sub-grid scheme calculates the geometry of a cloud, including the cloud base, the cloud top, and the cloud extent. These calculated sub-clouds are composed of air transported vertically and laterally between the cloud and the surrounding environment. Concentrations of pollutants for each layer of the cloud are calculated by Equation 2:

$$\bar{m}_i^{\text{cld}}(z) = f_{\text{ent}} \left[(1 - f_{\text{ent}}) \bar{m}_i^{\text{down}} + f_{\text{side}} \bar{m}_i(z) \right] + (1 - f_{\text{ent}}) \bar{m}_i^{\text{up}}, \quad (2)$$

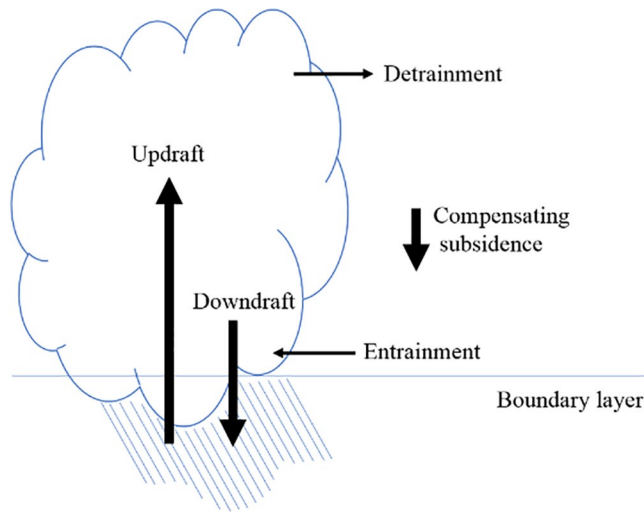


Figure 1. Schematic of cloud convection and the processes involved.

where f_{side} is the fraction of entrained air originating from the side of the cloud and f_{ent} is the entrainment calculated by iteratively solving both conservation and thermodynamic equations (Chang et al., 1987; Walcek & Taylor, 1986). \bar{m}_i^{down} represents the below cloud concentrations, and \bar{m}_i^{up} represents the above cloud concentrations. Once the cloud volume has been calculated, the average temperature, pressure, total water content, and pollutant concentrations are computed based on liquid water content W_c as the weighting function that assigns the most weight to the layers with the highest liquid water content. Thus, the average pollutant concentrations within clouds are calculated following Equation 3:

$$\bar{m}_i^{\text{cld}} = \frac{\int_{z_{\text{cbase}}}^{z_{\text{ctop}}} \bar{m}_i^{\text{cld}}(z) W_c(z) dz}{\int_{z_{\text{cbase}}}^{z_{\text{ctop}}} W_c(z) dz} \quad (3)$$

The final step of convective mixing is the reapportioning of the mass back into each individual layer. Although the cloud mixing of below cloud, above cloud, and within cloud layers varies, this step is accomplished by fractional cloud coverage, in-cloud initial and final concentrations, and the vertical concentration profile. The algorithm of the CMAQ scheme of

sub-grid clouds has resulted in improved efforts to parameterize the net effects of the displacement of air by the convection and subsidence of that air back into layers below the cloud. The mixing algorithm of CMAQ does not simulate the dynamic nature of air flows within the processes of convection.

2.2. The Structure of the KF-Convection Model

The KF module of a convective cloud that we presented and implemented uses a pattern of mixing that relies on a dynamic description of a cloud. Here, the estimation of pollutant concentrations is based on the physical processes of transporting air modeled from the WRF meteorological model.

To set up the main algorithm of the KF scheme in CMAQ, we first need mass flux variables and cloud properties from the WRF model to represent the convective processes of the cloud. A list of these variables appears in Table S1. The body of the convective mixing represented in the KF scheme is a mass-conserved steady-state entraining-detraining plume model. The concept of these mixing processes involves mass fluxes of updraft and downdraft among the layers of the convection cloud as the driving forces that vertically transport masses of air from the convection originating layer to the ending layer. It also includes two-way mass fluxes between the layers of cloud convection and the environment through entrainment and detrainment. Therefore, understanding the potential originating layers of updraft and downdraft and their ending layers is a necessary task that requires assessing and modifying the modules of the WRF model. We archived the KF cloud characteristics and transferred the required parameters listed in Table S1 into the CMAQ model through the coupling subroutines inside the WRF-CMAQ two-way system.

The main code for KF convective mixing follows the concept of the KF algorithm (Kain, 2004; Kain & Fritsch, 1990, 1993). The schematic of a cloud and the processes involved in convective mixing are presented in Figure 1. The main code begins by distinguishing the grid points where convection is taking place. We implement our scheme only for grid points with convection. Then we differentiate them into two categories of clouds, deep and shallow convection. Shallow convection is activated only when we have deep convection in which updraft is more shallow than the minimum cloud depth. This typically occurs at below 4 km, while deep convective clouds occur at 4 km and higher. The modeling of deep convection begins with the impacts of the updraft. The calculation of updraft considers the effects of upward fluxes of air masses from the updraft originating layer moving to its ending layers. Updraft calculations also take into account the mass fluxes of entrainment and detrainment in the middle layers. We finally include the effect of compensation distributed throughout the cloud layers.

Deep convection modeling continues with calculations related to the effects of the downdraft. The procedure follows the same algorithm of calculations that we conducted for the updraft, but it uses the downward

```

Algorithm: CONV KF
Define Cumulus convection variables
Get KF-scheme variables from WRF
  for i: 1 to NROWS
    for j: 1 to NCOLS
      if Deep convection is happening:
        Compute the updraft effect.
        Compute the entrainment-detrainment effect.
        Compute the effect of compensating due to updraft.
        Compute the downdraft effect.
        Compute the entrainment-detrainment effect.
        Compute the effect of compensating due to downdraft.
      else if Shallow convection is happening:
        Compute the updraft effect.
        Compute the entrainment-detrainment effect.
        Compute the effect of compensating due to updraft.
      End
    End
  End
Update the concentrations matrix
Continue to sub-grid cloud scheme
  
```

Figure 2. Pseudocode for the KF-convection module developed inside the CMAQ modeling system. CMAQ, Community Multiscale Air Quality; KF, Kain and Fritsch.

fluxes of air from the downdraft originating layer to the surface. It also contains the impacts of entrainment and detrainment fluxes between these layers and subsequently distributes the effects of compensation.

For cases of shallow convection, the KF main code calculates only the updraft effect, which involves the elements of the upwards fluxes of masses from the bottom to top layers of clouds, the impacts of mixing air through the entrainment and detrainment, and the compensating effect due to the updraft. At the last step of the deep and shallow cloud calculations, the KF would update concentrations of all of the required grid points of convection. The general pseudocode for this algorithm is presented in Figure 2.

The main differences between the Standard-CMAQ model and our developed KF-convection module according to what we have discussed above are presented in Table 1. Some key elements play significant roles in the algorithm of the KF-convection scheme, changing the transport of a pollutant species between the layers and over the modeling region. The main factors are temporal resolution, cloud geometry, transported air through the convective vertical layers, and convection classification. Using KF-convection for cloud geometry and mixing, we ensure the consistency of cloud parameterization between the chemical transport and meteorological models. This consistency benefits the convective transport

modeling of trace gases by taking into account real convective areas, direct convective fluxes, and accurate cloud geometries. It also helps prevent a mismatch between the convection fields and mass/moisture fields (Li et al., 2018).

3. Investigating the KF-Convection Impact in an Idealized Case

To validate the concept of KF-convection main code, first, we tested it in an idealized case, defined as a situation that has no interferences from physical and chemical processes (i.e., advection, diffusion, and aerosols chemistry) except KF-convection. The testing required KF-related tendencies and cloud information archived from a WRF output. In the next step, by implementing the main code for a specific vertical profile of a trace gas, CO, in this case, we investigate the impact of convective mixing on the vertical distribution of the pollutant. To achieve a more comprehensive understanding of the change, we implemented the process over 35 vertical layers (from the bottom to the top of the domain) in 10 synchronization time steps lasting a total of 60 min. The objective of this section was to represent the general concept of the KF-convection main code. To this end, we selected four cases: (a) deep convection with only updraft flux, (b) deep convection with only downdraft flux, (c) deep convection with both updraft and downdraft fluxes, and (d) shallow convection with updraft flux. In all of the cases, we accounted for the effect of entrainment, detrainment, also subsidence effect.

Table 1

Comparison Between the Main Parts of the Cloud Parameterization of the Standard-CMAQ Algorithm and the KF-Convection Algorithm

	Standard-CMAQ	KF-convection
	Sub-grid scheme	Cloud modeling
Temporal resolution	1 h	Synchronization time (~6 min)
Cloud geometry (definition of the cloud layers and characteristics)	CMAQ parameterization	Utilized the dynamic model (WRF)
Vertical mixing (air transporting by updraft and downdraft)	CMAQ parameterization	Developed model consistent with the dynamic meteorological model (WRF)
Convection classification	General cloud	Deep and shallow convection

CMAQ, Community Multiscale Air Quality; KF, Kain and Fritsch.

By investigating the differences between concentration profiles before and after applying KF-convection considering the flux rates, we observed that for the case of deep convection with only updraft (Figure 3a), the updraft flux moves the concentrations from the originating layer of updraft flux to the cloud's top layer. The minor impacts in between are caused by entrainment, detrainment, and subsidence effects. On the other hand, for the case of deep convection with the only downdraft (Figure 3b), the vertical profile of concentration after applying the KF-convection demonstrates how concentrations are reduced over upper layers and diffused into lower layers at the ending point of downdrafts. Also, both downdraft entrainment and detrainment strengthen the impact in this case. In the case where we include both updraft and downdraft in the deep convection (Figure 3c), we observe the combined impact of increasing concentrations in layers near the clouds top and the ending layers of the downdraft, as well as the decreasing concentration at the updraft originating and downdraft originating layers. Furthermore, the shallow convection case with updraft (Figure S1) has an impact similar to that of deep convection with updraft only. Although the overall impact of KF-convection fluxes seems to be marginal in the tested idealized case, in real cases, the impacts will be accumulated, and they will redistribute the vertical profiles of pollutants considerably.

4. Investigating the Impact of KF-Convection in a Real Case

4.1. Reference Setup

For the real case investigation, we applied WRF-CMAQ two-way coupled model (Wong et al., 2012). To prevent any impact from chemistry on meteorology, we turned off the feedback. We chose this model because it has the same structure as the WRF-CMAQ off-line modeling framework; in addition, it requires no extra preparation of the meteorological parameters for the CTM (running the Meteorology-Chemistry Interface Processor). Unlike the conventional off-line CMAQ model, in which calculations are driven by hourly meteorological data, the calculations of the WRF-CMAQ two-way coupled model occur in synchronous time steps (e.g., every 360 s, based on a run-time parameter), which we considered helpful in this case. After all, the convection model functions in smaller time steps from which we need to access variables.

The WRF and CMAQ model share a single domain with a 27 km horizontal grid spacing over East Asia, shown in Figure 4. The coupled model consists of WRF version 3.8 and CMAQ version 5.2. We set Morrison double-moment scheme for microphysics and the Rapid Radiative Transfer Model for GCMs scheme for longwave and shortwave radiation. We utilized the ACM2 planetary boundary layer (PBL) model (Pleim, 2007a, 2007b) and the Pleim-Xiu land surface model (Pleim & Xiu, 1995; Xiu & Pleim, 2001). The cumulus parameterization scheme employed in WRF had to be KF (Kain & Fritsch, 1990, 1993) to transfer the required variables. The initial and boundary conditions for meteorology were produced based on the National Centers for Environmental Prediction FNL (final) operational global analysis data. In addition, we employed Hemispheric CMAQ v5.3 to calculate initial and boundary conditions for chemistry. More information on the reference model setup and emission inventory can be found in Jung et al. (2021). Additionally, we adjusted the CO anthropogenic emissions of East Asia based on Tang et al.'s (2019) simulations. We conducted the simulation between April 20 and May 31, 2016, spent 10 days in April for model spin-up and studied May 2016 and the KORUS-AQ campaign days on which the convection impacted flight measurement areas.

4.2. Case Study: KORUS-AQ Aircraft Campaign

During the KORUS-AQ aircraft campaign measurements, we chose days with convection to further study the detailed roles of KF-convection on the performance of the CMAQ modeling system. The routes of selected KORUS-AQ flights and radar reflectivity in Figure S2 show the presence of convection during some flights in the area. We compared the developed KF-convection model with the Standard-CMAQ model for the days on which we observed convection over the aircraft measurement points by interpolating model outputs to observation points. Comparisons between measured and modeled concentrations of CO on all convection days showed that the application of the KF-convection module reduced the number of under- and over-predicted concentration points (Figure 5). According to the histogram difference of relative bias between two models and observations (see Figure S3), the KF-convection model reduced under-predicted points by ~550 and over-predicted points by ~100. Although the KF-convection model had a negative

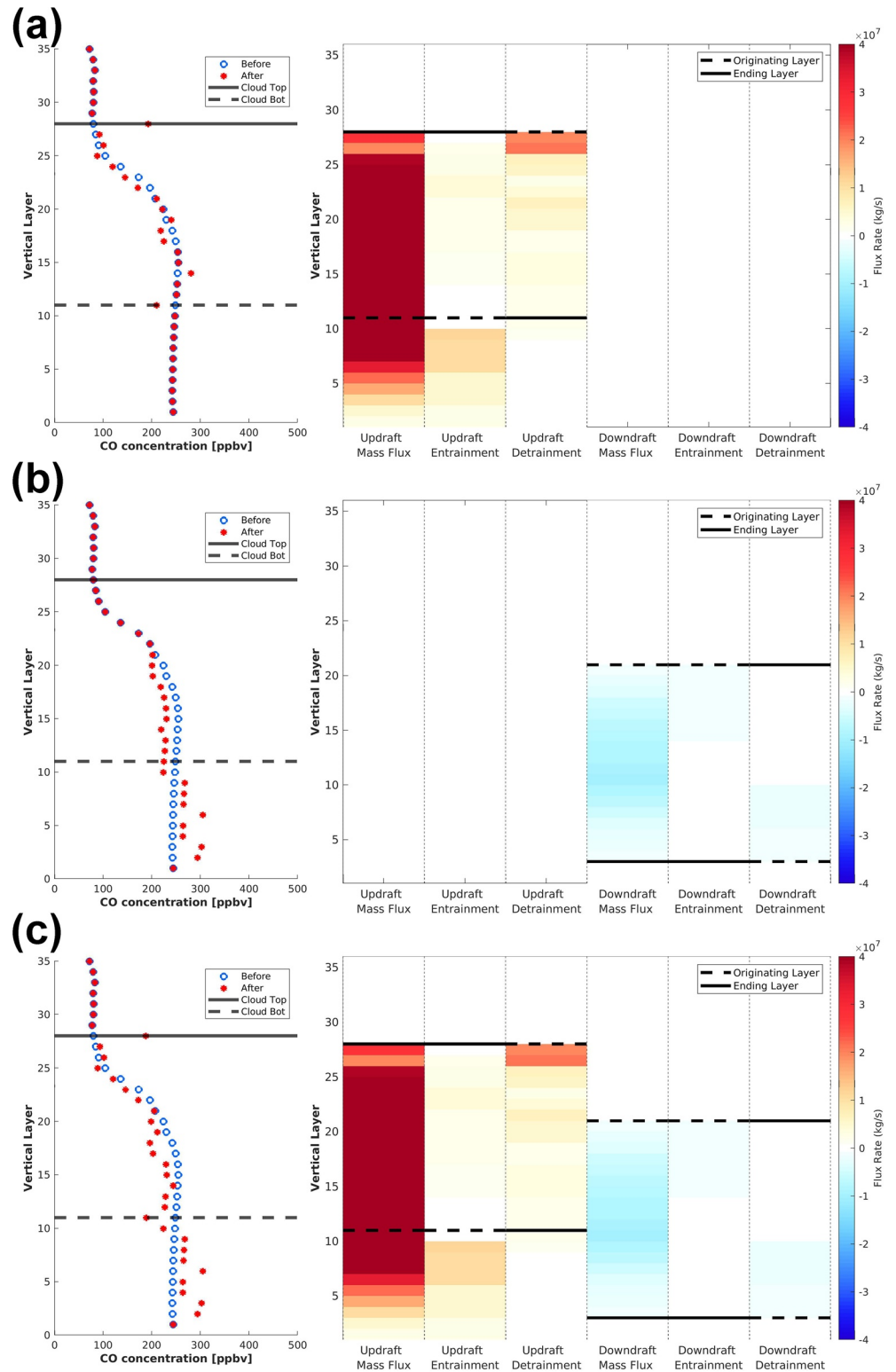


Figure 3. Comparison of the differences between the concentration profile (left) caused by KF-convection tendencies (right) for the cases of (a) deep convection with the updraft, (b) deep convection with downdraft, and (c) deep convection with both updraft and downdraft. KF, Kain and Fritsch.

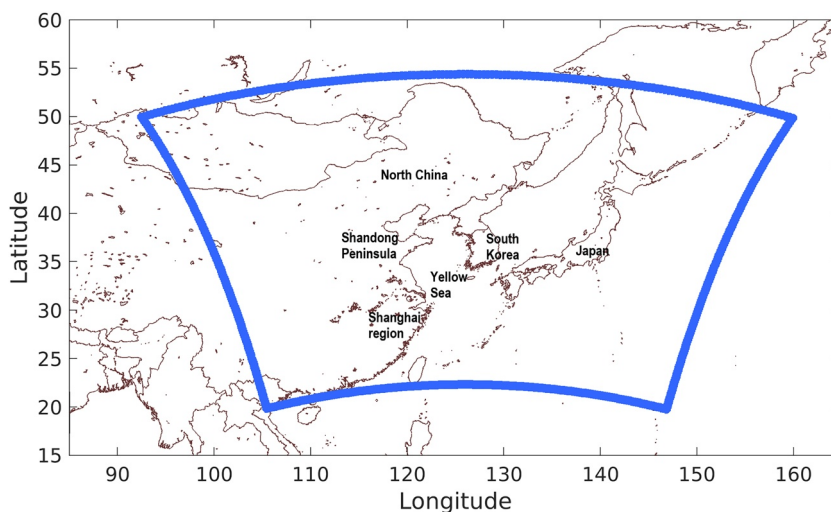


Figure 4. Map of the study region; the blue line indicates the study domain.

impact in some cases, the overall difference shown in the histograms indicates the large impact of KF-convection on reducing the number of under- and over-predicted points. Furthermore, we evaluated the statistical parameters for these two models at different altitude ranges (see Table S2). Basically, above the PBL (~0–2 km) and mid-tropospheric altitude, we found a higher correlation and index of agreement (IOA) when we compared the results. More specifically, over the lower mid-troposphere (~2–4 km), the KF-convection model predicts CO concentrations that are closer to concentrations measured by aircraft. However, over the surface and in the upper mid-troposphere (~4–6 km), the prediction becomes less accurate. Interestingly, after the modifications of KF-convection, the predictions of CO concentrations over the upper troposphere (~6–9 km) improved; the results can be caused by either direct impact of KF-convection over the area or by the tropospheric transport of increased concentrations caused by KF-convection in other regions. To view the impact of the KF-convection module spatially, we prepared horizontal plots of simulated CO concentrations for the KF-convection and Standard-CMAQ models compared to aircraft measurements

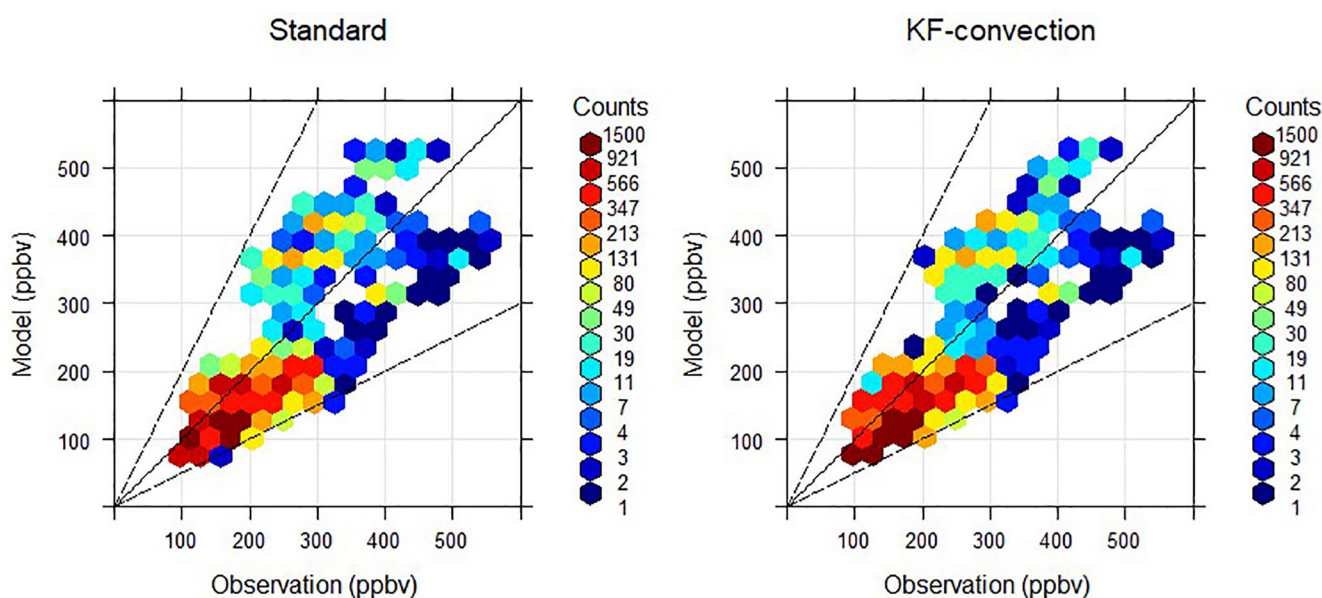


Figure 5. CO concentrations found by the model versus aircraft CO measurements for the Standard-CMAQ and CMAQ with the KF-convection model (the number of points in each bin is depicted by colors). CMAQ, Community Multiscale Air Quality; CO, carbon monoxide; KF, Kain and Fritsch.

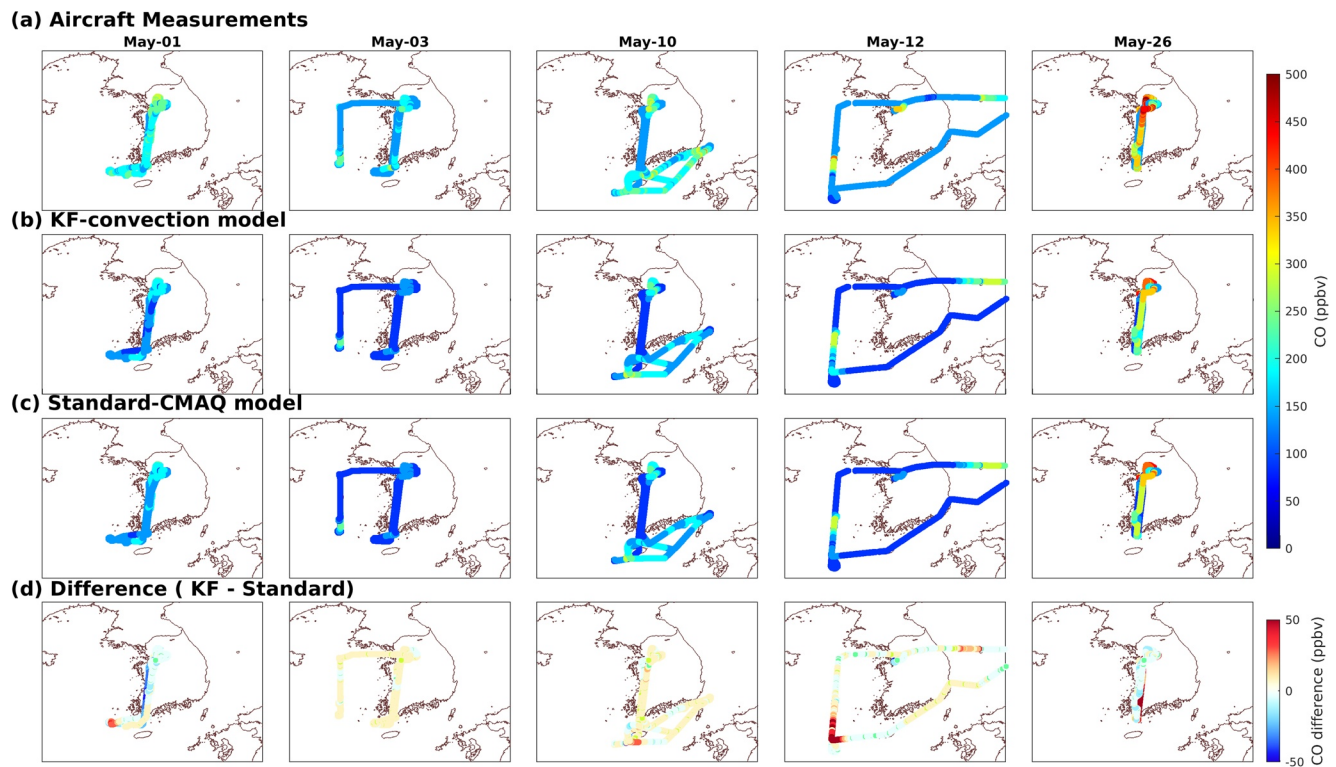


Figure 6. Spatial analysis of CO concentrations in aircraft tracks over South Korea on convection days: (a) Aircraft measurements, (b) The KF-convection model, (c) The Standard-CMAQ model, (d) The difference between the KF-convection and Standard-CMAQ models. CMAQ, Community Multiscale Air Quality; CO, carbon monoxide; KF, Kain and Fritsch.

over the track of aircraft during the convection days with all the measured points (Figure 6). We will address these findings in greater detail in the following sections.

To view the impact of the KF-convection module spatially, we prepared horizontal plots of simulated CO concentrations for the KF-convection and Standard-CMAQ models compared to aircraft measurements over the track of aircraft during the convection days with all the measured points. The model outputs were linearly interpolated to the exact location of the measurements. Overall we observed under-estimations from both models. The KF-convection module attempt to reduce this underestimation on May 3 and May 10. On other days, we see a mixed impact of the KF-convection module, an enhancement, and a reduction in CO concentrations. From panel (d), we identify the points with the largest differences. These points highly correlate with the radar reflectivity in that area (see Figure S2), indicating that the strongest impact of the KF-convection module occurs when the measurements are near or at the convection points. In Section 5, we will explain how and why the KF-convection module impacts CO concentrations.

4.3. Comparison With Satellite-Derived CO Columns

The scattered convective area around the measurements during KORUS-AQ days indicates the spatial impact on CO concentrations that the KF-convection module would produce over the region. Although this impact focuses on vertical mixing, minor differences that would change the patterns in CO transport over the region of study are expected to occur. To investigate these differences, we used the NASA Terra MOPITT version 8, level 2, multispectral total column retrievals with standard quality flags for comparison. We calculated the CO total column based on averaging kernels for the KF-convection and Standard-CMAQ models. Figure 7 panel (a) represents the MOPITT CO total column for the entire month of May 2016 and separately for each of the convection days (May 1, May 3, May 10, May 12, and May 26). Panels (b) and (c) represent the CO total column for the KF-convection and Standard-CMAQ models, respectively. To study the impact of the KF-convection module, we also plotted a map for each case that displayed the differences between the

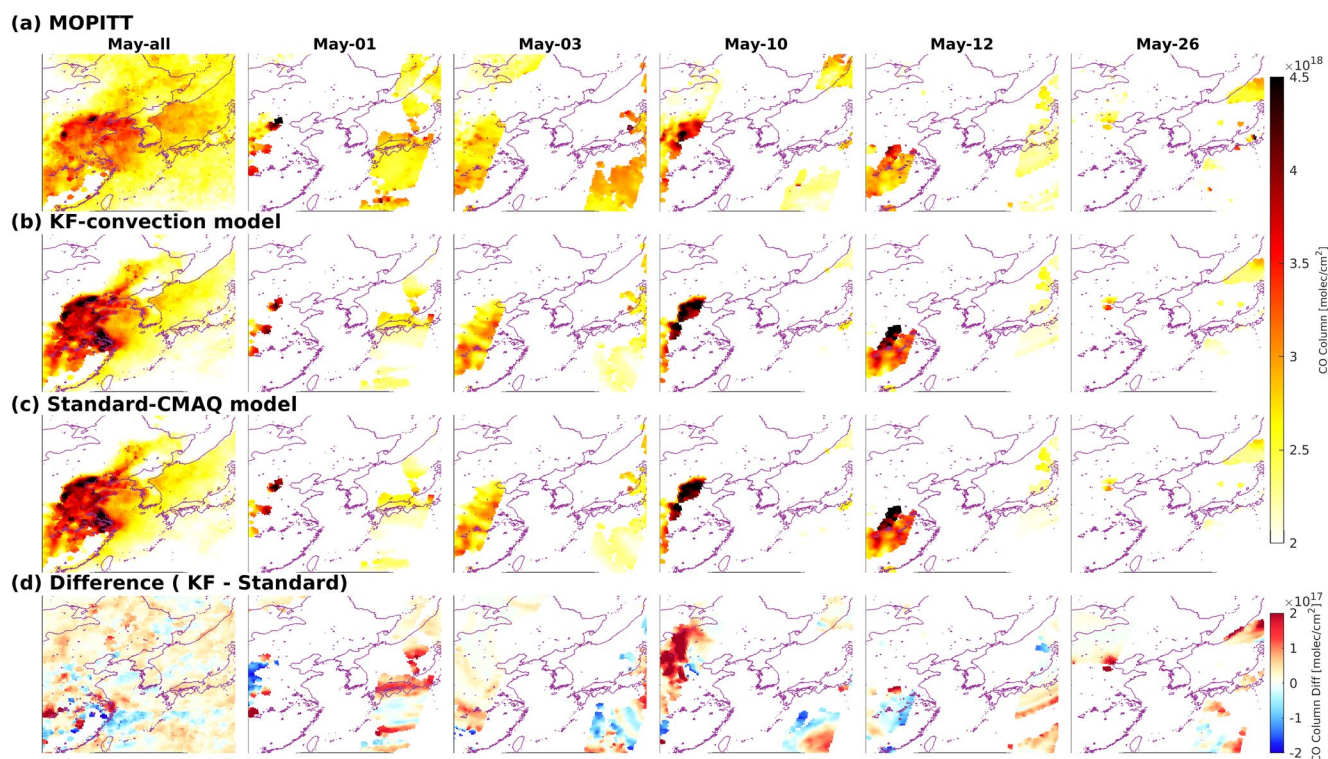


Figure 7. Spatial comparison of the total CO columns for the convection days in May 2016 (May-01, May-03, May-10, May-12, and May-26), averaged over the entire month (May-all), (a) the MOPITT measured total CO columns, (b) the KF-convection module simulated CO columns, (c) the Standard-CMAQ model simulated CO columns, and (d) the difference between the CO columns of the KF-convection and Standard-CMAQ models. CMAQ, Community Multiscale Air Quality; CO, carbon monoxide; KF, Kain and Fritsch.

KF-convection and Standard-CMAQ models (panel d). In general, the models over-estimate CO columns over China and the Yellow Sea. According to Table 2, the overall impact of KF-convection caused the model to generate marginally higher IOA for the averaged CO column over the entire month of May. As of May 1 and May 3, the IOA and correlation decreased marginally; the KF-convection module, however, reduced the mean bias and mean absolute error. For the remaining convection days, this module consistently reduced bias and increased the IOA. From panel (d), we observe a distinguishable impact on the east and west sides of the map on May 1 and May 10. Comparisons of the spatial distributions revealed that the KF-convection module alters the vertical mixing of the CO profiles, and the combination of mixing with horizontal transport could lead to considerable changes in CO transport patterns.

5. A Comparison Between the CMAQ With KF-Convection and Standard-CMAQ Models

Convection is the primary cause of the vertical mixing of tracers across cloud layers. In the atmosphere where both convection and advection simultaneously transport constituents to various altitudes and regions, differentiating between vertical mixing and horizontal transport is a complicated task. In this part of our study, we illustrate how KF-convection could impact CO concentrations over latitudes and longitudes of measurements during convection days. Such an impact could be due to the vertical mixing of CO pollutants across cloud layers. During the process of vertical mixing, which we refer to as the “direct impact of KF-convection,” intensive upward fluxes of convection help with lifting the CO concentrations from the updraft originating layer to the top layer of the cloud. An equally important process responsible for the difference between concentrations at any altitude, especially layers higher than 2 km, is the horizontal transport of CO. Tracers pushed to higher levels could be advected to another region. In this study, we refer to such an impact as the “indirect impact of KF-convection.” Thus, whereas the inquiry into the direct impact of KF-convection mostly focuses on vertical mixing caused by the KF scheme, the study of the indirect

Table 2
Statistical Analysis of the KF-Convection and Standard-CMAQ Modeled CO Column Versus the MOPITT CO Column for Convection Days in May 2016 (May-01, May-03, May-10, May-12, and May-26), Averaged Over the Entire Month of May 2016 (May-All)

		IOA	R	MAE	MB	RMSE
May-all	KF-convection	0.699666	0.818576	5.33E+17	-4.44E+17	6.85E+17
	Standard-CMAQ	0.69323	0.818883	5.45E+17	-4.61E+17	6.96E+17
May-01	KF-convection	0.515233	0.618245	7.04E+17	-6.85E+17	8.71E+17
	Standard-CMAQ	0.517034	0.639575	7.24E+17	-7.06E+17	8.71E+17
May-03	KF-convection	0.598759	0.796003	7.10E+17	-6.61E+17	8.74E+17
	Standard-CMAQ	0.600105	0.805933	7.11E+17	-6.67E+17	8.74E+17
May-10	KF-convection	0.653015	0.771208	7.01E+17	-5.67E+17	8.82E+17
	Standard-CMAQ	0.635949	0.764381	7.27E+17	-6.05E+17	9.21E+17
May-12	KF-convection	0.816427	0.841772	3.73E+17	-1.40E+17	5.24E+17
	Standard-CMAQ	0.814253	0.846377	3.93E+17	-1.56E+17	5.31E+17
May-26	KF-convection	0.503251	0.570847	6.35E+17	-5.75E+17	8.53E+17
	Standard-CMAQ	0.485646	0.558987	6.48E+17	-6.09E+17	8.63E+17

Note. In comparisons between the KF-convection model and satellite measurements, green indicates improvement by the KF-convection module, red indicates rosining by the model. (IOA, index of agreement; MAE, mean absolute error; MB, mean bias; R, correlation; RMSE, root mean square error).

impact is more general, focusing on the physical processes responsible for the differences caused by KF-convection. In the next sections, we will elaborate on both types.

5.1. Direct Impact of KF-Convection

It is generally believed that deep or shallow convection can efficiently inject air masses from the originating layers of updrafts over the PBL into the mid and upper-troposphere (Konopka et al., 2019). When we introduced our KF-convection scheme to the sub-grid clouds of CMAQ, the impact of the new approach changed the vertical mixing profile of CO concentrations. Figure 8 panel (a) shows the vertical profile of modeled CO concentrations from the KF-convection scheme compared with observation points of campaign flight for May 1, May 3, May 10, May 12, and May 26, the days and hours on which convection occurred. Figure 8 panel (b) shows the same comparison of modeled and observed concentrations for the Standard-CMAQ model. From these two panels, it is noticeable that on some days the CO concentrations have higher intensity over the surface. This is because flights measured concentrations at lower altitudes over the Seoul Metropolitan Area and the long-range transport of pollutants from China (Ghahremanloo et al., 2021; Mousavinezhad et al., 2021; Pouyaei et al., 2020). The colored points in panels (a) and (b) depict the aircraft measurement values for different ranges of altitudes. To take into account the contribution of KF-convection to the changes in CO concentrations over the measured points, we included the differences between the concentrations found by the CMAQ with KF-convection module and those found by the Standard-CMAQ model, shown in panel (c). The differences are shown in this panel lie within a range from -50 to +50 ppb. On some days (e.g., May 12 and May 26), the impacts of KF-convection on differences in concentrations are apparent while they are less on other days, shown in Figure 8c. To illustrate the causes of these differences, the up-

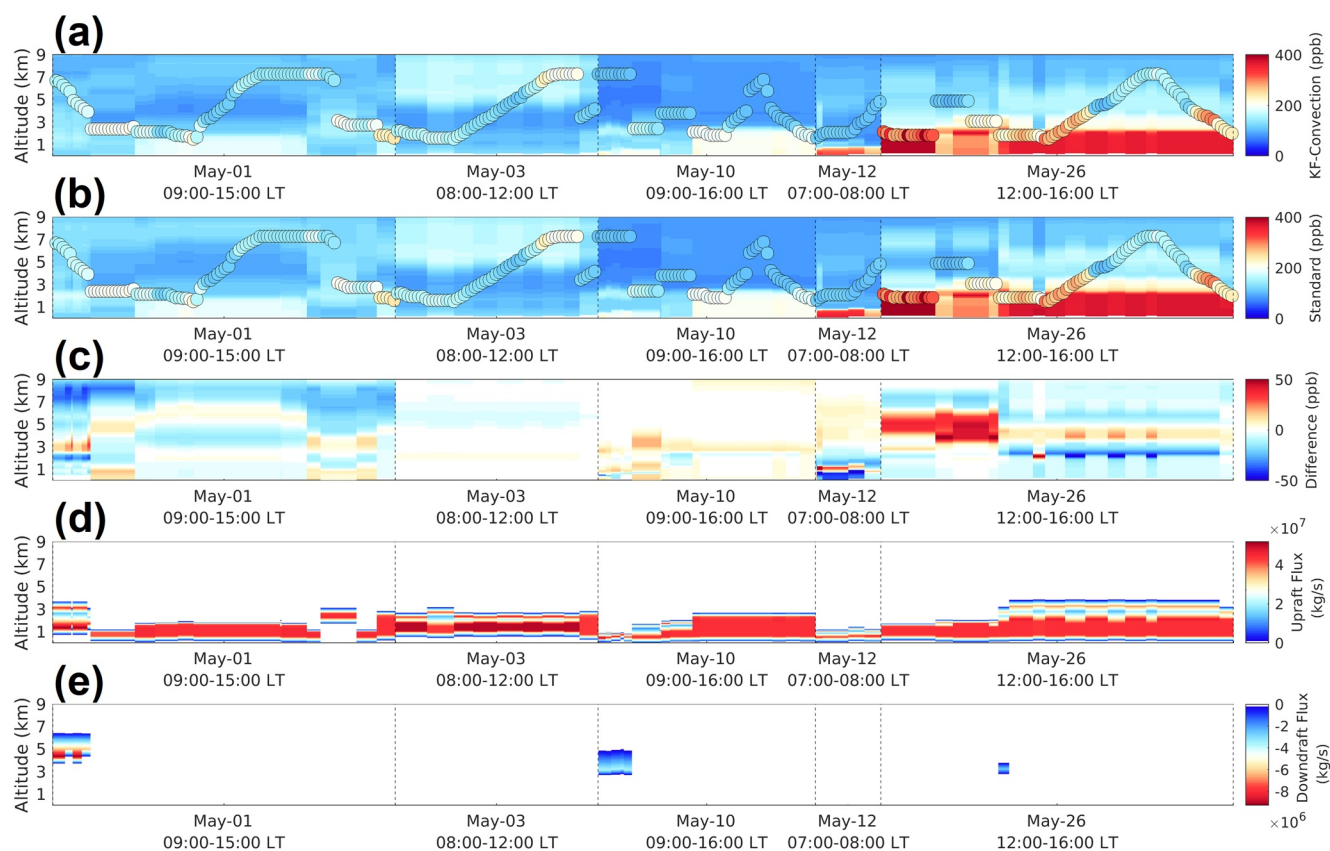


Figure 8. Analysis of the direct impact of KF-convection on days with convection: (a) CO concentrations determined by the KF-convection model at different altitude ranges versus CO measurements of DC8 aircraft (points); (b) CO concentrations determined by the Standard-CMAQ model at different altitude ranges versus CO measurements of DC8 aircraft (points); (c) differences between the CO concentrations of the CMAQ with KF-convection and Standard-CMAQ models; (d) the updraft flux rate at different altitudes from the KF-convection model; and (e) the downdraft flux rate at different altitudes from the KF-convection model. CMAQ, Community Multiscale Air Quality; CO, carbon monoxide; KF, Kain and Fritsch.

draft and downdraft flux rates from the KF-convection model during the exact point of measurements are shown in Figure 8 panels (d) and (e).

Figure 8 shows that in the early hours of measurements on May 1, the CO concentrations over the surface and lower altitudes (~1–2 km) were lifted to higher altitudes (~3–4 km) by updrafts. Conversely, downdrafts with sufficient counter-flux rate pushed down the concentrations, resulting in a small deficit in CO concentrations in the upper troposphere (~5–7 km). The CO concentration in the mid-day hours of May 1 exhibited mixed effects from both updraft flux at 3 km altitude and possible transport from other regions at higher altitude (~6–7 km). In the next section, we will elaborate the convective mixing and its relation to the transport of CO concentrations over the region of study. On May 3 and May 10, differences in CO concentrations were marginal but still noticeable, especially at 3 km and above, in increments of 10–20 ppbv. We can also spot a relatively small downdraft flux at the early hours of May 10, which did not cause a noticeable impact on CO concentrations. The situation, however, differed on May 12, when a 50 ppbv decrease in the CO concentration over the surface caused by KF-convection occurred along with a 40 ppbv increase at a 1-km altitude caused by high energy updraft flux. But on this day, in higher altitudes (>2 km), the decrement or increment of CO concentration must be caused by the indirect impact of KF-convection. The major cause of these differences around mid-day on May 26 at 3–6 km altitudes was the transport of CO originating in another region, which revealed itself in the KORUS-AQ campaign observation area. Conversely, the other differences in CO concentrations on May 26 can be explained by the direct impact of updraft flux, which we detected by comparing the patterns of differences in CO concentrations and those in the vertical profiles of updraft flux.

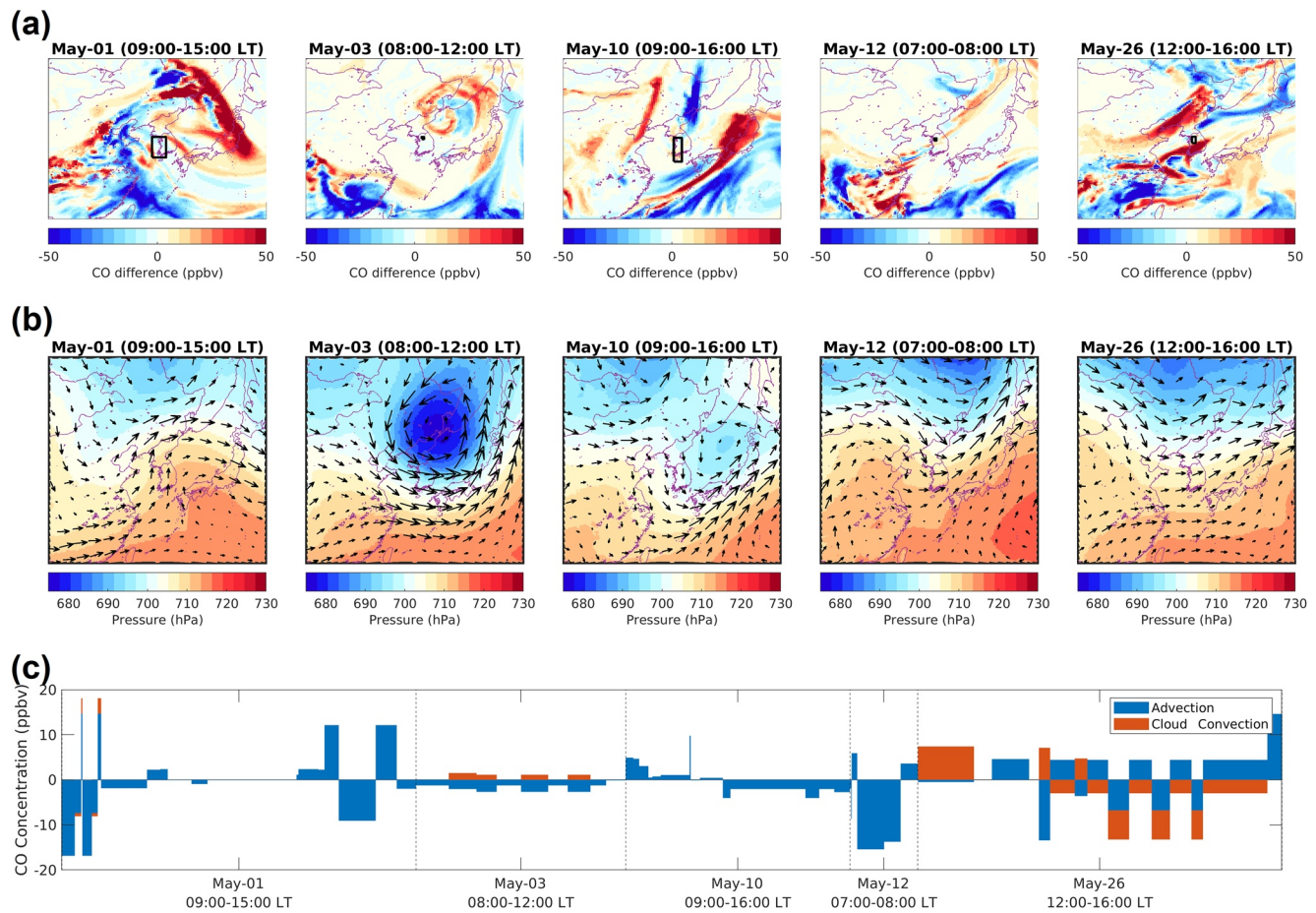


Figure 9. Analysis of the indirect impact of KF-convection on days with convection at 3 km altitude, (a) averaged spatial distribution of the differences between the CO concentrations from CMAQ with KF-convection module and those from the standard-CMAQ model over the study domain, (b) the averaged wind pattern and pressure field over the study domain, (c) results of the process analysis of the differences between the CMAQ with KF-convection and Standard-CMAQ models at the points where convection occurred. CMAQ, Community Multiscale Air Quality; CO, carbon monoxide; KF, Kain and Fritsch.

5.2. Indirect Impact of KF-Convection

As previously mentioned, another explanation for differences in CO concentrations at observation points is the indirect impact of KF-convection. For this purpose, we examined the spatial distribution of CO concentration differences, taking into account the maps of wind patterns and pressure fields over the region of study. We also differentiated the physical processes responsible for differences in CO concentrations involved in the model through the application of the PA module, an integrated process rate approach in CMAQ modeling. To thoroughly evaluate the impacts of the KF scheme on the distribution of CO over the region, we examined two altitudes: the mid-troposphere (3 km) and the lower troposphere (1 km). We also provided the same plots for the upper troposphere (6 km) in the supporting information.

Figure 9 panel (a) shows the spatial distribution of differences in CO concentrations, calculated by the results of the Standard-CMAQ model subtracted from the results of the CMAQ with KF-convection module at an altitude of 3 km on convection days over the domain of study. The black lines indicate the area around campaign observations on each day of measurements. Figure 9 panel (b) shows the wind patterns and pressure fields at the same altitude (3 km), and Figure 9 panel (c) represents the PA results of the CO concentration differences for two responsible processes of advection (i.e., the indirect impact) and cloud convection (i.e., the direct impact) for the exact points where convection occurred.

The difference among the distributions of CO concentrations at the 3 km altitude during May 1 observation hours shows two patterns of CO concentrations: a decreased difference in CO concentrations over East

China and an increased difference over the regions north of the Korean Peninsula and the Sea of Japan. The mentioned patterns of CO differences stem from both the direct and indirect impacts of KF-convection that we introduced earlier. The direct impact of KF-convection was mainly due to fluxes of updrafts and downdrafts, which played an influential role in each vertical layer of the cloud by changing total masses of air within each layer. In contrast, the indirect impact of KF-convection appears to have originated from horizontal winds transporting masses of air to hundreds of kilometers across the region of the study. A mixture of direct and indirect impacts of KF-convection shows reasonable agreement with that shown in the meteorological map on May 1. Primarily south-westerly wind patterns transported the updated masses of air from the more industrialized areas of China toward the Korean Peninsula and Japan at an altitude layer of 3 km. Results from the PA module for this day reveal that the contribution from cloud convection (i.e., the direct impact of KF-convection) was marginal. During morning hours, however, advection contributed about -10 ppbv, which we regarded as a sink for CO difference concentration, but in the afternoon, the contribution from advection was positive or negative, around ± 10 ppbv.

Plots from May 3 indicate that KF cloud convection contributed to a lower degree of positive differences above the Korean Peninsula and the Sea of Japan during the presence of a cyclone. Strong patterns of wind components around the cyclone caused a more homogeneous atmospheric layer over the Korean Peninsula. The weakening patterns of wind speed show relatively more level of CO differences, probably because of the direct impacts of KF-convection. Overall, the direct and indirect impacts of KF-convection on May 3, compared to other days, were marginal. The spatial difference in CO levels also indicates the marginal difference common over the Korean Peninsula. Interestingly, although the wind pattern for May 3 was relatively strong and north-westerly since the net amount of CO difference caused by KF-convection was marginal in the north-western part of the Korean Peninsula, this strong wind pattern caused marginal, if any, differences in CO in the measurement points.

The maps of wind pattern for May 10 and May 12 follow a relatively similar form of south-westerly horizontal wind components. On both days, the wind pattern was in favor of transport of CO concentrations caused by KF-convection from south-eastern China toward the western regions of the Korean Peninsula. In particular, on May 10, when positive differences in CO concentration were demonstrably higher over Japan, the strong south-westerly wind appeared to influence the transport of the CO constituents to this region. The map of CO difference also shows that patterns of low-speed winds are indicative of the presence of stagnant air with positive differences in CO levels. The negative difference in CO concentrations over the northern part of the Korean Peninsula was developed by the loss of masses of air that could have been due to the transport of species through the help of northerly winds. These masses of air could have changed the distributions of CO concentration over the region of the measurement campaign in the black rectangle. Again, it is worthwhile to mention that these discrepancies were the result of a mixture of both direct and indirect impacts of the KF-convection. The results of the integrated process rate also show the mixed positive and negative contribution of CO concentration for this day. On the other hand, on May 12, the distinguishable plume over the Shanghai region and the Yellow Sea was responsible for the transport of CO concentrations toward the South Korea region. From the results of the PA, we conclude that the impact from concentrations of this plume was negative and that advection was a major sink on this day.

May 26 represents a special case among the measurement days. The results of PA on this day indicate that the absolute amount of cloud convection was equal to or higher than that of advection. To be more concise, the average spatial distribution of the difference in CO concentrations at 3 km altitude showed intensive positive and negative impacts from KF-convection from China over the Yellow Sea to the Korean Peninsula. Two separate plumes of air impacted CO concentrations over the target region; one from the Shanghai region with mostly positive and some negative differences in CO levels (± 50 ppbv) and one from the Shandong Peninsula with all positive differences ($+40$ ppbv). The wind pattern also favored long-range transport from China toward the Korean Peninsula. Interestingly, during the first hours of measurements, although the average wind pattern was westerly, the contribution of cloud convection (i.e., the direct impact of KF-convection) was positive, indicating that updrafts were the major source of changes in CO levels over the target area during this period. However, after an hour or two, the contribution of cloud convection exhibited mixed responses from being a source to being a sink weighted toward sinking. In most cases, cloud convection had a negative impact, explained by the updrafts at a 3 km altitude that lifted the constituents

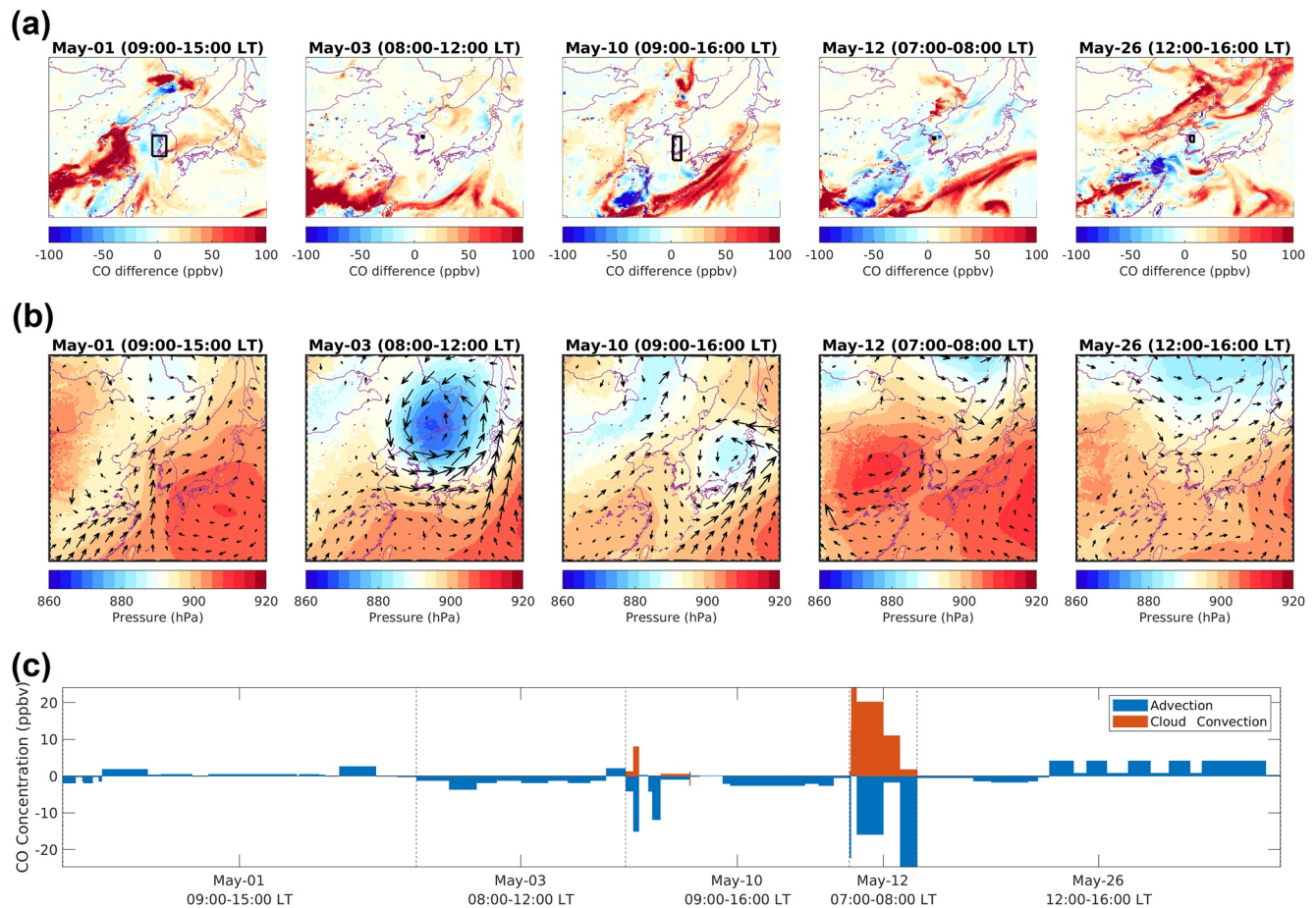


Figure 10. Analysis of the indirect impact of KF-convection for days with convection at a 1-km altitude: (a) averaged spatial distribution of the differences between the CO concentrations from the KF-convection and Standard-CMAQ models over the study domain, (b) average wind patterns and pressure fields over the study domain, (c) results of the process analysis for the differences between the CO concentrations from the KF-convection and Standard-CMAQ models at the points where convection occurred. CMAQ, Community Multiscale Air Quality; CO, carbon monoxide; KF, Kain and Fritsch.

of CO and led to negative differences in CO concentrations; and in some cases, the altitudes of the updrafts were lower than 3 km, which positively impacted differences in CO levels. Advection also showed a mixed response, from positive to negative, caused by plumes moving toward the target region.

We also prepared plots of the indirect impact analysis at a 1-km altitude and reviewed the extent to which differences between CO concentrations could be attributed to cloud convection at this altitude (Figure 10). On May 1 and May 3, the overall impact on these differences was marginal in the area of measurements. The PA results show differences in concentrations of less than ± 3 ppbv. In addition, the spatial distribution of these differences did not reflect any significant transport of CO from highly polluted areas toward the target region. Although the wind patterns followed the same direction as winds at 3 km altitude, the magnitude was noticeably smaller, so the severity of the transport was lower. The wind pattern and pressure distribution map for May 10 shows a relatively stagnant condition over the Korean Peninsula, which explains why the transport-related impact was mostly local. From the spatial distribution of concentrations, we also spot some negative differences in CO around the target area, which confirms the results of the PA analysis finding negative CO concentrations from advection. The positive impact of cloud convection in the early morning of May 10 corresponds to the updraft flux at lower altitudes, which we saw in Figure 8 panel (d). When the altitude of the updraft flux is lower, the impact of the cloud convection is more apparent. Following the same logic, the highly positive CO concentrations from cloud convection (i.e., the direct impact) on May 12 were caused by intense low-altitude updrafts, represented in Figure 8 panel (d). In addition, the differences in the negative plumes of CO over the target region explained the sinking effect of the advection process.

On May 26, however, KF-convection had no significant impact at a 1-km altitude. The indirect impact of KF-convection at the 6 km altitude (see Figure S4) was consistent with our findings for 3 and 1 km altitudes; that is, the higher the altitude, the greater the impact of advection or transport from other regions.

6. Conclusion

The complete and realistic modeling of convective mixing in unresolved clouds is of great importance in CTMs. This study implemented a version of the KF scheme into the CMAQ cloud module to present a physically more realistic convective mixing of chemical compounds and provide a fully consistent approach with cloud parameterization in a meteorological model. The developed KF-convection scheme separates shallow and deep convection. Based on their physical nature, the scheme accounts for updraft flux, downdraft flux, entrainment, detrainment, and the subsiding effect. To validate our approach, we verified the process of convective mixing in several cases with updraft and downdraft. Then, we tested our developed convection module for CO concentrations over East Asia during the KORUS-AQ campaign period to investigate its impact on differences in concentrations. We first compared the results over aircraft measurement points statistically and spatially. Then, we investigated the impact on the CO column by comparing the results with the MOPITT CO column. Then we analyzed the impact of KF-convection from two perspectives: One mostly focused on the vertical profiles of CO concentrations and the other considering the CO spatial distribution over the domain of study. We referred to these perspectives as the direct and indirect impact of KF-convection, respectively.

An investigation of both types of impacts revealed the potential of KF-convection to substantially increase or decrease CO concentrations over the domain of study at different altitudes. In the early hours of May 1, the updrafts and downdrafts played a significant role in increasing and decreasing CO concentrations at various altitudes. The differences which occurred during the rest of the day were primarily caused by the indirect effect of KF-convection through transport. On May 3 and May 10, the major process responsible for differences in CO levels at 3 km altitude was cloud convection and advection respectively. The overall impact of KF-convection, however, was low. May 12 showed a negative plume of CO difference from China at higher altitudes but a direct impact of updraft fluxes below PBLH. Finally, on May 26, updrafts increased CO concentrations at higher altitudes, and advection influenced the CO concentrations over the region. Investigating KF-convection impact at 1 km altitude showed a similar response as 3 km altitude. However, we noticed that intensive lower altitude fluxes were responsible for differences in CO concentration levels on convection days.

We concluded that the KF-convection scheme has a clear impact when applied to the sub-grid cloud module in CMAQ. The inclusion of the KF scheme as a complete and independent sub-grid cloud module inside CMAQ, however, requires further investigation. By implementing the same study for ozone, NO₂, and water vapor and comparing such distributions with observations, we plan to investigate the impact of KF-convection on the vertical distribution of other species in the mid-troposphere and study the impact of aqueous chemistry and wet deposition.

Data Availability Statement

The data set used for evaluation of the models was downloaded from the KORUS-AQ data repository (<https://doi.org/10.5067/Suborbital/KORUSAQ/DATA01>, KORUS-AQ—An International Cooperative Air Quality Field Study in Korea, 2016), and the MOPITT-derived CO columns were downloaded from EARTH-DATA website (https://doi.org/10.5067/TERRA/MOPITT/MOP02J_L2.008, MOPITT Derived CO [Near and Thermal Infrared Radiances] V008). The CMAQ model is an open-source model that can be accessed via Zenodo (<https://doi.org/10.5281/zenodo.1167892>, US EPA Office of Research and Development, 2017). The idealized case for KF-convection and the WRF-CMAQ Two-way model with the KF-convection module can be accessed via Zenodo (<https://doi.org/10.5281/zenodo.4724239>, Pouyaei, 2021).

Acknowledgments

This study was supported by the FRIEND (Fine Particle Research Initiative in East Asia Considering National Differences) Project through the National Research Foundation of Korea (NRF) funded by the Ministry of Science and ICT (2020M3G1A1114619). Dr. Chun Zhao was supported by the Fundamental Research Funds for the Central Universities, the National Natural Science Foundation of China (Grant number 41775146), and the Strategic Priority Research Program of Chinese Academy of Sciences (Grant number XDB41000000). This study was completed, in part, with resources provided by the Research Computing Data Core at the University of Houston.

References

- Alapaty, K., Herwehe, J. A., Otte, T. L., Nolte, C. G., Bullock, O. R., Mallard, M. S., et al. (2012). Introducing subgrid-scale cloud feedbacks to radiation for regional meteorological and climate modeling. *Geophysical Research Letters*, *39*(24), L24809. <https://doi.org/10.1029/2012GL054031>
- Arakawa, A. (2004). The cumulus parameterization problem: Past, present, and future. *Journal of Climate*, *17*(13), 2493–2525. [https://doi.org/10.1175/1520-0442\(2004\)017<2493:RATCPP>2.0.CO;2](https://doi.org/10.1175/1520-0442(2004)017<2493:RATCPP>2.0.CO;2)
- Barth, M. C., Kim, S.-W., Wang, C., Pickering, K. E., Ott, L. E., Stenchikov, G., et al. (2007). Cloud-scale model intercomparison of chemical constituent transport in deep convection. *Atmospheric Chemistry and Physics*, *7*(18), 4709–4731. <https://doi.org/10.5194/acp-7-4709-2007>
- Bechtold, P., Bazile, E., Guichard, F., Mascart, P., & Richard, E. (2001). A mass-flux convection scheme for regional and global models. *Quarterly Journal of the Royal Meteorological Society*, *127*(573), 869–886. <https://doi.org/10.1002/qj.49712757309>
- Bogenschutz, P. A., Gettelman, A., Morrison, H., Larson, V. E., Schanen, D. P., Meyer, N. R., & Craig, C. (2012). Unified parameterization of the planetary boundary layer and shallow convection with a higher-order turbulence closure in the Community Atmosphere Model: Single-column experiments. *Geoscientific Model Development*, *5*(6), 1407–1423. <https://doi.org/10.5194/gmd-5-1407-2012>
- Byun, D., & Schere, K. L. (2006). Review of the governing equations, computational algorithms, and other components of the models-3 Community Multiscale Air Quality (CMAQ) modeling system. *Applied Mechanics Reviews*, *59*(1–6), 51–76. <https://doi.org/10.1115/1.2128636>
- Chandra, N., Venkataramani, S., Lal, S., Sheel, V., & Pozzer, A. (2016). Effects of convection and long-range transport on the distribution of carbon monoxide in the troposphere over India. *Atmospheric Pollution Research*, *7*(5), 775–785. <https://doi.org/10.1016/j.apr.2016.03.005>
- Chang, J. S., Brost, R. A., Isaksen, I. S. A., Madronich, S., Middleton, P., Stockwell, W. R., & Walcek, C. J. (1987). A three-dimensional Eulerian acid deposition model: Physical concepts and formulation. *Journal of Geophysical Research*, *92*(D12), 14681. <https://doi.org/10.1029/JD092iD12p14681>
- Chapman, E. G., Gustafson, W. I., Easter, R. C., Barnard, J. C., Ghan, S. J., Pekour, M. S., & Fast, J. D. (2009). Coupling aerosol-cloud-radiative processes in the WRF-Chem model: Investigating the radiative impact of elevated point sources. *Atmospheric Chemistry and Physics*, *9*(3), 945–964. <https://doi.org/10.5194/acp-9-945-2009>
- Dennis, R. L., McHenry, J. N., Barchet, W. R., Binkowski, F. S., & Byun, D. W. (1993). Correcting RADM's sulfate underprediction: Discovery and correction of model errors and testing the corrections through comparisons against field data. *Atmospheric Environment Part A: General Topics*, *27*(6), 975–997. [https://doi.org/10.1016/0960-1686\(93\)90012-N](https://doi.org/10.1016/0960-1686(93)90012-N)
- Erukhimova, T., & Bowman, K. P. (2006). Role of convection in global-scale transport in the troposphere. *Journal of Geophysical Research*, *111*(D3), D03105. <https://doi.org/10.1029/2005JD006006>
- Ervens, B. (2015). Modeling the processing of aerosol and trace gases in clouds and fogs. *Chemical Reviews*, *115*(10), 4157–4198. <https://doi.org/10.1021/cr5005887>
- Fahey, K. M., Carlton, A. G., Pye, H. O. T., Baek, J., Hutzell, W. T., Stanier, C. O., et al. (2017). A framework for expanding aqueous chemistry in the Community Multiscale Air Quality (CMAQ) model version 5.1. *Geoscientific Model Development*, *10*(4), 1587–1605. <https://doi.org/10.5194/gmd-10-1587-2017>
- Fowler, L. D., Barth, M. C., & Alapaty, K. (2020). Impact of scale-aware deep convection on the cloud liquid and ice water paths and precipitation using the Model for Prediction across Scales (MPAS-v5.2). *Geoscientific Model Development*, *13*(6), 2851–2877. <https://doi.org/10.5194/gmd-13-2851-2020>
- Fritsch, J. M., & Chappell, C. F. (1980). Numerical prediction of convectively driven mesoscale pressure systems. Part I: Convective parameterization. *Journal of the Atmospheric Sciences*, *37*(8), 1722–1733. [https://doi.org/10.1175/1520-0469\(1980\)037<1722:NPOCDM>2.0.CO;2](https://doi.org/10.1175/1520-0469(1980)037<1722:NPOCDM>2.0.CO;2)
- Ghahremanloo, M., Lops, Y., Choi, Y., & Mousavinezhad, S. (2021). Impact of the COVID-19 outbreak on air pollution levels in East Asia. *Science of the Total Environment*, *754*, 142226. <https://doi.org/10.1016/j.scitotenv.2020.142226>
- Ghude, S. D., Beig, G., Kulkarni, P. S., Kanawade, V. P., Fadnavis, S., Remedios, J. J., & Kulkarni, S. H. (2011). Regional co pollution over the Indian-subcontinent and various transport pathways as observed by mopitt. *International Journal of Remote Sensing*, *32*(21), 6133–6148. <https://doi.org/10.1080/01431161.2010.507796>
- Grell, G., Freitas, S. R., Stuefer, M., & Fast, J. (2011). Inclusion of biomass burning in WRF-Chem: Impact of wildfires on weather forecasts. *Atmospheric Chemistry and Physics*, *11*(11), 5289–5303. <https://doi.org/10.5194/acp-11-5289-2011>
- Heikenfeld, M., Marinescu, P. J., Christensen, M., Watson-Parris, D., Senf, F., Heever, van den, S. C., & Stier, P. (2019). tobac 1.2: Towards a flexible framework for tracking and analysis of clouds in diverse datasets. *Geoscientific Model Development*, *12*(11), 4551–4570. <https://doi.org/10.5194/gmd-12-4551-2019>
- Herwehe, J. A., Alapaty, K., Spero, T. L., & Nolte, C. G. (2014). Increasing the credibility of regional climate simulations by introducing subgrid-scale cloud-radiation interactions. *Journal of Geophysical Research*, *119*(9), 5317–5330. <https://doi.org/10.1002/2014JD021504>
- Jung, J., Choi, Y., Wong, D. C., Nelson, D., & Lee, S. (2021). Role of sea fog over the yellow sea on air quality with the direct effect of aerosols. *Journal of Geophysical Research: Atmospheres*, *126*(5), e2020JD033498. <https://doi.org/10.1029/2020JD033498>
- Kain, J. S. (2004). The Kain-Fritsch convective parameterization: An update. *Journal of Applied Meteorology*, *43*, 170–181. [https://doi.org/10.1175/1520-0450\(2004\)043<0170:TKCPAU>2.0.CO;2](https://doi.org/10.1175/1520-0450(2004)043<0170:TKCPAU>2.0.CO;2)
- Kain, J. S., & Fritsch, J. M. (1990). A one-dimensional entraining/detraining plume model and its application in convective parameterization. *Journal of the Atmospheric Sciences*, *47*(23), 2784–2802. [https://doi.org/10.1175/1520-0469\(1990\)047<2784:AODEPM>2.0.CO;2](https://doi.org/10.1175/1520-0469(1990)047<2784:AODEPM>2.0.CO;2)
- Kain, J. S., & Fritsch, J. M. (1993). Convective parameterization for mesoscale models: The Kain-Fritsch scheme. In *The representation of cumulus convection in numerical models* (pp. 165–170). American Meteorological Society. https://doi.org/10.1007/978-1-935704-13-3_16
- Konopka, P., Tao, M., Ploeger, F., Diallo, M., & Riese, M. (2019). Tropospheric mixing and parametrization of unresolved convective updrafts as implemented in the chemical lagrangian model of the stratosphere (CLaMS v2.0). *Geoscientific Model Development*, *12*(6), 2441–2462. <https://doi.org/10.5194/gmd-12-2441-2019>
- Lawrence, M. G., & Rasch, P. J. (2005). Tracer transport in deep convective updrafts: Plume ensemble versus bulk formulations. *Journal of the Atmospheric Sciences*, *62*(8), 2880–2894. <https://doi.org/10.1175/JAS3505.1>
- Li, Y., Pickering, K. E., Barth, M. C., Bela, M. M., Cummings, K. A., & Allen, D. J. (2018). Evaluation of parameterized convective transport of trace gases in simulation of storms observed during the DC3 field campaign. *Journal of Geophysical Research: Atmospheres*, *123*(19), 11261–11238. <https://doi.org/10.1029/2018JD028779>
- Mousavinezhad, S., Choi, Y., Pouyaei, A., Ghahremanloo, M., & Nelson, D. L. (2021). A comprehensive investigation of surface ozone pollution in China, 2015–2019: Separating the contributions from meteorology and precursor emissions. *Atmospheric Research*, *257*, 105599. <https://doi.org/10.1016/j.atmosres.2021.105599>
- Ong, H., Wu, C., & Kuo, H. (2017). Effects of artificial local compensation of convective mass flux in the cumulus parameterization. *Journal of Advances in Modeling Earth Systems*, *9*(4), 1811–1827. <https://doi.org/10.1002/2017MS000926>

- Orbe, C., Waugh, D. W., Yang, H., Lamarque, J., Tilmes, S., & Kinnison, D. E. (2017). Tropospheric transport differences between models using the same large-scale meteorological fields. *Geophysical Research Letters*, *44*(2), 1068–1078. <https://doi.org/10.1002/2016GL071339>
- Park, M., Randel, W. J., Emmons, L. K., & Livesey, N. J. (2009). Transport pathways of carbon monoxide in the Asian summer monsoon diagnosed from Model of Ozone and Related Tracers (MOZART). *Journal of Geophysical Research*, *114*(8), D08303. <https://doi.org/10.1029/2008JD010621>
- Pleim, J. E. (2007a). A combined local and nonlocal closure model for the atmospheric boundary layer. Part I: Model description and testing. *Journal of Applied Meteorology and Climatology*, *46*(9), 1383–1395. <https://doi.org/10.1175/JAM2539.1>
- Pleim, J. E. (2007b). A combined local and nonlocal closure model for the atmospheric boundary layer. Part II: Application and evaluation in a mesoscale meteorological model. *Journal of Applied Meteorology and Climatology*, *46*(9), 1396–1409. <https://doi.org/10.1175/JAM2534.1>
- Pleim, J. E., & Xiu, A. (1995). Development and testing of a surface flux and planetary boundary layer model for application in mesoscale models. *Journal of Applied Meteorology*, *34*(1), 16–32. <https://doi.org/10.1175/1520-0450-34.1.16>
- Pouyaei, A. (2021). *CMAQ-Twoway-KF-convection*. Zenodo. <https://doi.org/10.5281/zenodo.4724239>
- Pouyaei, A., Choi, Y., Jung, J., Sadeghi, B., & Song, C. H. (2020). Concentration trajectory route of air pollution with an integrated Lagrangian model (C-TRAIL model v1.0) derived from the Community Multiscale Air Quality Modeling (CMAQ model v5.2). *Geoscientific Model Development Discussions*, *13*, 1–30. <https://doi.org/10.5194/gmd-2019-366>
- Randall, D. A., Wood, R. A., Bony, S., Colman, R., Fichefet, T., Fyfe, J., et al. (2007). *Climate models and their evaluation, climate change 2007: The physical science basis. Contribution of working group I to the fourth assessment report of the intergovernmental panel on climate change*. Cambridge University Press.
- Roselle, S. J., & Binkowski, F. S. (1999). *Cloud dynamics and chemistry*. Retrieved from http://cmasceneter.org/cmaq/science_documentation/pdf/ch11.pdf
- Saito, K., Fujita, T., Yamada, Y., Ishida, J. I., Kumagai, Y., Aranami, K., et al. (2006). The operational JMA nonhydrostatic mesoscale model. *Monthly Weather Review*, *134*(4), 1266–1298. <https://doi.org/10.1175/MWR3120.1>
- Sakradzija, M., & Klocke, D. (2018). Physically constrained stochastic shallow convection in realistic kilometer-scale simulations. *Journal of Advances in Modeling Earth Systems*, *10*(11), 2755–2776. <https://doi.org/10.1029/2018MS001358>
- Samuelsson, P., Jones, C. G., Willén, U., Ullerstig, A., Gollvik, S., Hansson, U., et al. (2011). The Rossby Centre Regional Climate model RCA3: Model description and performance. *Tellus Series A Dynamic Meteorology and Oceanography*, *63*(1), 4–23. <https://doi.org/10.1111/j.1600-0870.2010.00478.x>
- Scott, B. C. (1981). Sulfate washout ratios in winter storms. *Journal of Applied Meteorology*, *20*(6), 619–625. [https://doi.org/10.1175/1520-0450\(1981\)020<0619:SWRIWS>2.0.CO;2](https://doi.org/10.1175/1520-0450(1981)020<0619:SWRIWS>2.0.CO;2)
- Seinfeld, J., & Pandis, S. (2016). *Atmospheric chemistry and physics: From air pollution to climate change*. John Wiley & Sons.
- Skamarock, W. C., Klemp, J. B., Dudhia, J., Gill, D. O., Barker, D. M., Wang, W., & Powers, J. G. (2005). *A description of the advanced research WRF version 2*. Retrieved from <https://apps.dtic.mil/dtic/tr/fulltext/u2/a487419.pdf>
- Stocker, T. F., Qin, D., Plattner, G.-K., Tignor, M. M. B., Allen, S. K., Boschung, J., et al. (2013). *Climate change 2013 the physical science basis working group I contribution to the fifth assessment report of the intergovernmental panel on climate change*. Retrieved from www.cambridge.org
- Tang, W., Emmons, L. K., Arellano, A. F., Gaubert, B., Knote, C., Tilmes, S., et al. (2019). Source contributions to carbon monoxide concentrations during KORUS-AQ based on CAM-chem model applications. *Journal of Geophysical Research: Atmospheres*, *124*(5), 2796–2822. <https://doi.org/10.1029/2018JD029151>
- Tsai, W.-M., & Wu, C.-M. (2017). The environment of aggregated deep convection. *Journal of Advances in Modeling Earth Systems*, *9*(5), 2061–2078. <https://doi.org/10.1002/2017MS000967>
- US EPA Office of Research and Development. (2017) *CMAQ*. <https://doi.org/10.5281/ZENODO.1167892>
- Walcek, C. J., & Taylor, G. R. (1986). A theoretical method for computing vertical distributions of acidity and sulfate production within cumulus clouds. *Journal of the Atmospheric Sciences*, *43*(4), 339–355. [https://doi.org/10.1175/1520-0469\(1986\)043<0339:ATMFCV>2.0.CO;2](https://doi.org/10.1175/1520-0469(1986)043<0339:ATMFCV>2.0.CO;2)
- Wallace, J., & Hobbs, P. (2006). *Atmospheric science: An introductory survey* (Vol. 92). Elsevier.
- Wong, D. C., Pleim, J., Mathur, R., Binkowski, F., Otte, T., Gilliam, R., et al. (2012). WRF-CMAQ two-way coupled system with aerosol feedback: Software development and preliminary results. *Geoscientific Model Development*, *5*(2), 299–312. <https://doi.org/10.5194/gmd-5-299-2012>
- Wu, X., & Li, X. (2008). A review of cloud-resolving model studies of convective processes. *Advances in Atmospheric Sciences*, *25*(2), 202–212. <https://doi.org/10.1007/s00376-008-0202-6>
- Xiu, A., & Pleim, J. E. (2001). Development of a land surface model. Part I: Application in a mesoscale meteorological model. *Journal of Applied Meteorology*, *40*, 192–209. [https://doi.org/10.1175/1520-0450\(2001\)040<0192:doalsm>2.0.co;2](https://doi.org/10.1175/1520-0450(2001)040<0192:doalsm>2.0.co;2)
- Yang, B., Wang, M., Zhang, G. J., Guo, Z., Qian, Y., Huang, A., & Zhang, Y. (2020). Simulated precipitation diurnal variation with a deep convective closure subject to shallow convection in community atmosphere model version 5 coupled with CLUBB. *Journal of Advances in Modeling Earth Systems*, *12*(7). <https://doi.org/10.1029/2020MS002050>
- Yang, B., Zhou, Y., Zhang, Y., Huang, A., Qian, Y., & Zhang, L. (2018). Simulated precipitation diurnal cycles over East Asia using different CAPE-based convective closure schemes in WRF model. *Climate Dynamics*, *50*(5–6), 1639–1658. <https://doi.org/10.1007/s00382-017-3712-z>
- Zhao, C., Chen, S., Leung, L. R., Qian, Y., Kok, J. F., Zaveri, R. A., & Huang, J. (2013). Uncertainty in modeling dust mass balance and radiative forcing from size parameterization. *Atmospheric Chemistry and Physics*, *13*(21), 10733–10753. <https://doi.org/10.5194/acp-13-10733-2013>
- Zhao, C., Wang, Y., Choi, Y., & Zeng, T. (2009). Summertime impact of convective transport and lightning NO_x production over North America: Modeling dependence on meteorological simulations. *Atmospheric Chemistry and Physics*, *9*(13), 4315–4327. <https://doi.org/10.5194/acp-9-4315-2009>